

Ultrahigh-field quantitative MR imaging of ex vivo intracranial atherosclerotic plaques

Anita A. Harteveld¹, Nerissa P. Denswil², Jeroen C.W. Siero¹, Jaco J.M. Zwanenburg^{1,3}, Aryan Vink⁴, Wim G.M. Spliet⁴, Nikki Dieleman¹, Peter R. Luijten¹, Mat J.A.P. Daemen², Jeroen Hendrikse¹, and Anja G. van der Kolk¹

¹Department of Radiology, University Medical Center Utrecht, Utrecht, Netherlands, ²Department of Pathology, Academic Medical Center, Amsterdam, Netherlands,

³Image Science Institute, University Medical Center Utrecht, Utrecht, Netherlands, ⁴Department of Pathology, University Medical Center Utrecht, Utrecht, Netherlands

Introduction: Intracranial atherosclerosis is one of the most important causes of ischemic stroke and transient ischemic attack (TIA)¹. In the recent years, several intracranial vessel wall imaging techniques using (ultra)high-field magnetic resonance imaging (MRI) have emerged for the evaluation of atherosclerotic vessel wall lesions. However, a thorough correlation of MRI results of intracranial plaques with histopathology is still lacking^{2,3}. Quantitative MRI measurements may provide specific information of the NMR tissue properties of different atherosclerotic plaque components. This will allow for differentiation between those components. To investigate whether the various plaque components identified with MRI correspond to real histological differences within the plaque, a validation between MRI and histology is required. The purpose of this study was to investigate the ability of 7.0 tesla (7T) MRI to quantify different components within a plaque. Therefore, a multi-contrast ultrahigh-resolution MRI protocol at 7T was developed for *ex vivo* quantitative intracranial atherosclerotic plaque characterization.

Methods: Seven anonymous circle of Willis (CoW) specimens with a large atherosclerotic plaque burden were selected for this study. The specimens included the major arteries of the CoW. All specimens were cleaned from clotted blood products and embedded in a petri dish containing 2% agarose solution. Cactus spines were used as fiducials and placed at 15 locations of histological sampling, to enable spatial correlation with histology. The embedded specimens were scanned on a 7T whole body system (Philips Healthcare), with a home-made 16-channel dedicated surface coil, and a volume transmit/receive coil for transmission (Nova Medical). A scan protocol containing sequences with different contrast weightings was used to image the specimens from which the quantitative MR parameter maps were calculated. To obtain the quantitative T_1 , T_2 and PD maps, acquisition was performed at two specific flip angles according to the DESPOT1 and DESPOT2 method⁴. T_2^* maps were obtained using a dual-echo 3D T_2^* -weighted scan. The following scan parameters were used: DESPOT1 sequence, Field-of-view (FOV) 150x150x19.9mm³, acquired resolution 0.13x0.13x0.13mm³, TR/TE 26/4.3ms, flip angles (FA) 11 and 44 degrees, matrix size 1152x1154, bandwidth (BW) 165.1 Hz, 4 dynamic scans, TFE factor 1154; DESPOT2 sequence, FOV 150x150x19.9mm³, acquired resolution 0.13x0.13x0.13mm³, TR/TE 36/18ms, FA 12 and 62 degrees, matrix size 1152x1152, BW 40.5 Hz, 3 dynamic scans, TFE factor 1152; T_2^* map sequence, FOV 150x150x19.9mm³, acquired resolution 0.13x0.13x0.13mm³, TR/TE1/TE2 53/6.2/25.7ms, FA 29 degrees, matrix size 1152x1154, BW 101.3 Hz, NSA 1, TFE factor 1154. Total scan time was approximately 19h45min. To mitigate potential artifacts caused by scanner frequency drift, the scanner resonance frequency was measured and adjusted during scanning. For the balanced DESPOT2 the resonance frequency was increased by 9.2 Hz per dynamic scan, to shift the banding artifacts, and, thus avoid artifacts in the calculated T_2 maps. The dynamic scans with different RF offset frequencies were combined using a root-mean-square approach. Subsequent to the MR imaging of the specimen, samples were taken from the 15 marked locations for histological evaluation. The samples were placed in Ethylenediaminetetraacetic acid (EDTA) for three days to dissolve wall calcifications, to reduce the risk of damaging the specimen during sectioning, and stained with hematoxylin and eosin (HE) and elastic-Van Gieson (EVG). Based on the identified plaque components in a histological slide, regions of interest (ROIs) were drawn within the corresponding regions in the MR parameter maps to calculate the mean T_1 , T_2 , PD and T_2^* values for those regions.

Results: In the quantitative maps, several distinct areas corresponding to different atherosclerotic plaque components could be identified within the atherosclerotic plaques (Figure 1+2). The mean and standard deviation of T_1 , T_2 , PD and T_2^* values were calculated from the quantitative maps based on the plaque components identified in the histological slides (Table 1).

Conclusion: The presented ultrahigh-resolution MR imaging protocol enables quantitative analysis of the intracranial arterial vessel wall and concomitant plaques in *ex vivo* CoW specimen. Together with the results of the histological data, it may be possible to perform a proper correlation of the MRI findings with the underlying pathology to validate atherosclerotic plaque components. Furthermore, once it is known which plaque components can be identified with the presented quantitative MRI sequences, a translation can be made to *in vivo* intracranial vessel wall MR imaging by developing sequences based on the NMR tissue properties of the identified atherosclerotic plaque components.

References: ¹Arenillas JF, Stroke 2011; ²Kim JM, et al. Arch Neurol 2012; ³Qiao Y, et al. J Magn Reson Imaging 2011; ⁴Deoni SCL, et al. Magn Reson Med 2003

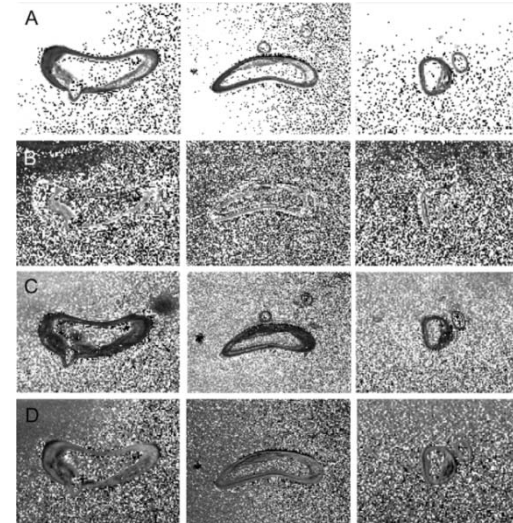


Figure 1. Quantitative T_1 (A), T_2 (B), T_2^* (C) and PD (D) maps at 7T of a cross section of the left vertebral artery in a CoW specimen embedded in 2% agarose solution. Different atherosclerotic plaque components can be identified within the atherosclerotic plaque. Left column: transverse plane; middle column: coronal plane; right column: sagittal plane.

Table 1. Mean \pm standard deviation of T_1 , T_2 , T_2^* and PD values of different components identified in the histological slide shown in figure 1. ROIs were drawn in the MR parameter maps at the location of the histologically identified tissue components. ^aNormalized to 'non-atherosclerotic' vessel wall present in the same slide.

Components	T_1 (ms)	T_2 (ms)	T_2^* (ms)	PD ^a
Lipid accumulation in plaque	420 \pm 177	44 \pm 33	11 \pm 5	0.82 \pm 0.37
Fibroid tissue in plaque	259 \pm 72	60 \pm 24	13 \pm 9	0.95 \pm 0.34
Vessel wall	139 \pm 49	48 \pm 27	20 \pm 10	1.13 \pm 0.46

Table 1. Mean \pm standard deviation of T_1 , T_2 , T_2^* and PD values of different components identified in the histological slide shown in figure 1. ROIs were drawn in the MR parameter maps at the location of the histologically identified tissue components. ^aNormalized to 'non-atherosclerotic' vessel wall present in the same slide.

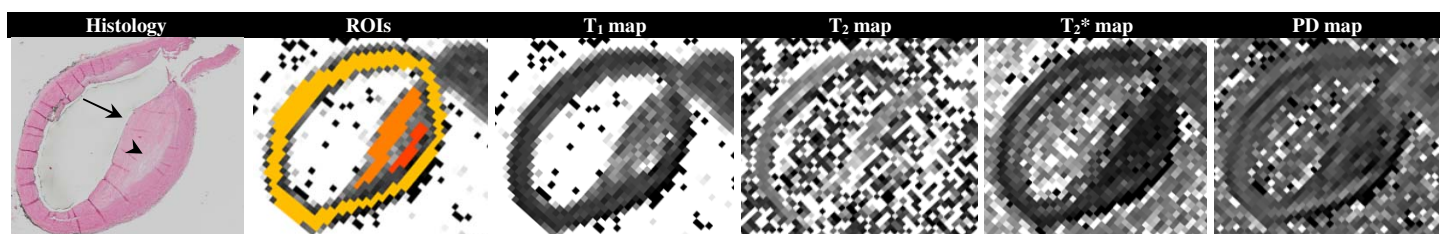


Figure 2. Histological slide (HE staining) of a sample taken from one of the circle of Willis specimen at the location of an atherosclerotic plaque in the left vertebral artery, with the corresponding calculated T_1 , T_2 , T_2^* , and PD maps. Regions of interest (ROIs) were drawn at the location of different tissue components identified in the histological slide to calculate the mean T_1 , T_2 , T_2^* and PD values for those regions (red ROI: lipid accumulation in plaque; orange ROI: fibroid tissue in plaque; yellow ROI: vessel wall). Arrow: thickened intima with atherosclerotic plaque; arrowhead: lipid accumulation within the plaque.